Radioprotectant screening for cryocrystallography

Robert J. Southworth-Davies and Elspeth F. Garman*

Laboratory of Molecular Biophysics, Department of Biochemistry, Rex Richards Building, South Parks Road, Oxford OX1 3QU, UK. E-mail: elspeth@biop.ox.ac.uk

Radiation damage continues to present a problem to crystallographers using cryocooled protein crystals at third-generation synchrotrons. Free-radical scavengers have been suggested as a possible means of reducing the rate of this damage. The screening of a large number of potential radioprotectants was undertaken with an online microspectrophotometer using cystine and cysteine to model protein disulfide bonds and thiol groups, respectively. Oxidized α-lipoic acid was tested as a possible model disulfide bond. The evidence for the effectiveness of ascorbate as a radioprotectant was strengthened, and quinone, 2,2,6,6-tetramethyl-4-piperidone, and reduced dithiothreitol showed promise as radioprotectants.

Keywords: radioprotectants; radiation damage; macromolecular cryocrystallography.

1. Introduction

The problem of radiation damage in cryocooled protein crystals has emerged recently as an important area of research for structural biologists. A disadvantage of X-rays as a probe is the energy they deposit through their inelastic interactions with matter, leading to radiation damage in macromolecular crystallography (MX). Radiation damage can be classified as primary or secondary in nature. Primary damage (which cannot be avoided) is the ionization of an atom by an X-ray photon through photoelectric absorption or Compton scattering. Secondary damage (dependent on the crystal chemistry and amenable to modification by experiment) is due to the formation of up to 500 secondary electrons, with mean track lengths of a few micrometres (for 12 keV photons), that will induce further excitation and ionization events within the atoms of the crystal (O'Neill et al., 2002). Together, these types of radiation damage are a limiting factor in taking X-ray measurements because, as radiation damage increases, the intensity of the diffraction pattern fades, initially with the loss of the higher-resolution reflections. This manifestation of a decrease in crystal order is a result of the significant movement of some atoms. We note that this loss of diffraction is an indirect rather than a direct measure of the radiation damage. In addition, site-specific structural damage occurs (Burmeister, 2000; Ravelli & McSweeney, 2000; Weik et al., 2000) so that the biological knowledge extracted from the model is potentially compromised (Owen et al., 2006).
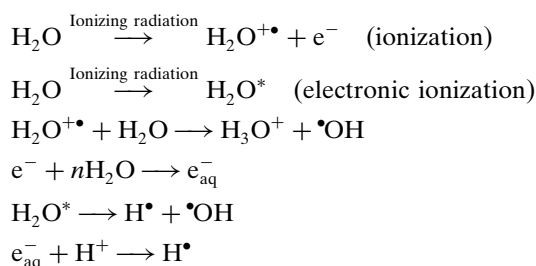
Damage by X-rays and other forms of ionizing radiation to organic materials was found by electron spin resonance (ESR) to proceed through the generation and propagation of free radicals (Swartz & Swartz, 1983). A free radical is any species capable of independent existence that contains one or more unpaired electrons (Halliwell & Gutteridge, 1999). In general, such a species is energetically unstable, and therefore free radicals tend to react very quickly, resulting in a product where the original free radical has lost its unpaired electron and formed a new radical species (chain reaction), or adds another free radical to form a complete pair (termination reaction). In some cases free radicals and other reactive species have been shown to play a role in the damage mechanism (Berges et al., 2000; Burmeister, 2000; Ravelli & McSweeney, 2000; Weik et al., 2002). Berges et al. (2000) examined disulfide bond cleavage in peptides and proteins at room temperature experimentally (one-electron reduction by $COO^{\bullet-}$ radicals and measurement of the resulting chain lengths) using two different theoretical approaches based on quantum chemistry and topology. Burmeister (2000), Ravelli & McSweeney (2000) and Weik et al. (2002) have discussed possible radical chemistry occurring in protein crystals at cryotemperatures.

Macromolecular crystals are routinely flash-cooled to, and held at, 100 K during most X-ray diffraction experiments in order to suppress secondary radiation damage caused by thermally mobile radicals (Hope, 1988; Garman & Schneider, 1997; Rodgers, 1997; Garman, 1999). Radiation damage still occurs in cryocooled proteins and was first described by Gonzalez et al. (1992) and further studied by Gonzalez & Nave (1994). Site-specific radiation-induced structural changes within cryocooled protein crystals were reported by several researchers in 2000. This specific damage was observed to occur to particular amino acids in a well defined order: first, the rupture of the disulfide bonds, followed by decarboxylation of glutamic and aspartic acid residues, the loss of OH from tyrosine residues and then the breakage of the C—S bond in methionines (Ravelli & McSweeney, 2000; Weik et al.,

radiation damage

2000; Burmeister, 2000; O'Neill *et al.*, 2002). The well defined order of susceptibility indicates that there must be some radical species causing secondary damage which are still mobile at 100 K. If they were not mobile, then specific damage would be observed at atoms with the largest X-ray absorption cross sections (*i.e.* the damage would be primary), or for atoms with high interaction cross sections with the resulting photo-electrons. This, in the absence of any heavier atoms, would give a susceptibility order of disulfide bonds followed by methionine residues, which is found not to be the case.

During X-ray exposure the incoming X-ray photon interacts with both the solvent (largely water) and protein molecules. Studies of the importance of water in biological radiation damage at room temperature were initiated by Powers *et al.* (1957). The interaction with the solvent is expected to produce various species with known yields [given in parentheses as G values, defined as the number of molecules changed per 100 eV absorbed (Ward, 1988)]: hydroxyl radicals (2.4), hydrated electrons (e_{aq}^-) (2.8), protons, hydrogen radicals (0.4) and hydrogen gas (0.4), through the reactions shown below:

$$H_2O \xrightarrow{\text{Ionizing radiation}} H_2O^{+\bullet} + e^- \quad \text{(ionization)}$$

$$H_2O \xrightarrow{\text{Ionizing radiation}} H_2O^* \quad \text{(electronic ionization)}$$

$$H_2O^{+\bullet} + H_2O \longrightarrow H_3O^+ + {}^\bullet OH$$

$$e^- + nH_2O \longrightarrow e_{aq}^-$$

$$H_2O^* \longrightarrow H^\bullet + {}^\bullet OH$$

$$e_{aq}^- + H^+ \longrightarrow H^\bullet$$

The hydroxyl radical is extremely labile, undergoing reactions with most organic molecules at a rate limited only by the rate of diffusion (Swartz & Swartz, 1983). Its favoured reaction is hydrogen-atom abstraction from nitrogen atoms of the backbone amides (Rao & Hayon, 1974). In the protein there are positively charged holes arising from the ejection of electrons, as well as negatively charged radicals. According to the ESR measurements of Jones *et al.* (1987), at liquid-nitrogen temperature (77 K) the positively charged holes are rapidly trapped, forming amido radicals on the protein backbone chain, whereas the electrons ejected by ionizing radiation have significant mobility. Rao *et al.* (1983) found that electrons added to proteins at 77 K can move efficiently within the protein until they encounter S—S bonds. In the absence of such bonds, and of other groups with high electron affinity, they remain in the protein until they are trapped at amide linkages. Other work on radical mobility also found that electrons are mobile at 100 K, and electron tunnelling in proteins has been reported to occur at temperatures as low as 5 K (Dick *et al.*, 1998); protons are known to become mobile in amorphous ice only at ~115 K (Fischer & Devlin, 1995); hydrogen gas has been detected emanating from amorphous solid water at 100 K following electron bombardment (Petrik & Kimmel, 2003); and $^\bullet$OH created in the solvent area of the crystal by the radiolysis of water are trapped at 100 K in ice crystals (Symons, 1999).

Following the observations of specific damage, attributable to secondary radiative effects, interest has grown in the possibility of using a variety of experimental strategies to try to mitigate it (reviewed by Garman, 2003). Here we report investigations on whether the addition of radioprotectants could prolong crystal lifetime by neutralizing immobile ionized groups or quenching radical species. These reagents can be incorporated into the lattice by soaking or co-crystallization. Radioprotectants are defined as compounds that either react with secondary radicals before they have a chance to damage the protein (*i.e.* they reduce indirect damage), or by interacting with the already damaged residue in such a way as to repair it to a predamaged state before further damaging reactions can occur (O'Neill *et al.*, 2002). In contrast, radical scavengers are defined as compounds which reduce indirect damage by reacting with an externally produced radical that could have subsequently inflicted damage if it had reached the protein. Radioprotectants are known to prevent damage to DNA in solution (Fulford *et al.*, 2001) and have acknowledged utility in the field of radiation chemistry as 'spin traps' (Lagercrantz, 1971).

For protein crystals at room temperature, the first attempt to use a free-radical scavenger to mitigate radiation damage was made by Zaloga & Sarma (1974), who soaked 2–30 mM styrene into radiation-sensitive immunoglobin crystals. This extended the resolution from 5.5 Å to 4 Å and gave a tenfold increase in the effective crystal lifetime (Zaloga & Sarma, 1974; Sarma & Zaloga, 1975). However, at increased concentrations of styrene, diffraction quality deteriorated due to polymerization of the styrene. Cascio *et al.* (1984) found that by replacing the native mother liquor with comparable solutions which contained in addition 10–20% by weight polyethylene glycol (PEG) of molecular weight 4000 or 20000, there was a reduction in radiation damage to the crystals tested. These crystals included firstly α-amylase protein crystals from pig pancreas where 20 h of exposure to 1.54 Å X-rays from an Elliot GX-20 rotating-anode generator caused a decline in intensity of 90% for reflections with spacings in the range 3.0–2.5 Å. After addition of 12% PEG 20000 to the mother liquor, crystals withstood exposure to the X-ray beam for 90 h before showing decay in the intensity pattern of no more than 10%. Secondly, the rhombohedral crystal form of canavalin from jack bean had a lifetime of 20 h or less in the X-ray beam, showing declines in average intensity of greater than 50%. When 15% PEG 4000 was added to the mother liquor, the crystals were stable for 80 h in the X-ray beam before suffering an average intensity decay of 10% or less. Thirdly, rabbit liver fructose 1,6-diphosphatase would undergo a 50% loss of overall intensity after 24 h of exposure to X-ray beam, but when 20% PEG 4000 was added to the mother liquor the radiation damage to the crystals was diminished by almost a factor of four. However, since we saw no radioprotectant effect for PEG (see §4), we suggest that the effects observed for PEG may possibly have been due to a polymerization effect or dehydration (the authors do not report the unit cells) rather than scavenging.

Following this early work on potential scavengers at room temperature, little was done to further the investigations. The advent of third-generation synchrotrons with high-brilliance beams, in which radiation damage is observed even at cryo-temperatures (around 100 K), has instigated new interest in the possibility of using radioprotectants as a means of trying to mitigate secondary radiation damage. Recently, Murray & Garman (2002) investigated styrene and ascorbate as potential radioprotectants at 100 K, concluding that styrene was ineffective whereas ascorbate showed potential. Further to this, Betts (2004) soaked 0.5 M ascorbate for 12 h into influenza virus N9 neuraminidase crystals to assess its radioprotective capacity on a 'real life' protein system. By inspecting electron density maps of the nine disulfide bonds in N9 calculated from sequential data sets, it was found that ascorbate protected residues on the outside of the protein but not those situated on the inside of the hollow ball formed by 24 N9 molecules in the I432 crystals. This result suggested a lack of penetration of ascorbate molecules into the solvent trapped inside the balls. Glucose was also soaked (for 30 min, as a 12 h soak significantly reduced diffraction) into N9 neuraminidase crystals at 0.5 M, but was shown to be totally ineffective as a radioprotectant and may even have exacerbated the radiation damage (Betts, 2004). Very recently, evidence has been published that nicotinic acid and 5,5′-dithiobis-2-nitrobenzoic acid can act as effective free-radical scavengers for MX (Kauffmann et al., 2006).

Various radical scavenging agents have been suggested and utilized in other fields such as extended X-ray absorption fine structure (EXAFS) (George et al., 1998), and electron microscopy where sugars are used as a protective matrix that quenches free radicals (Massover, 2006), but these have varying suitability for X-ray protein crystallography experiments. For instance, the transition metals (Halliwell & Gutteridge, 1999) and transition metal complexes such as $FeCN_6^{3-}$ could potentially act as radioprotectants in protein crystals (Jones et al., 1987; George et al., 2003), but the presence of such metal ions in the concentrations necessary for effective scavenging would increase the dose absorbed by the crystal significantly. The estimated time to reach the Henderson dose limit of 2×10^7 Gy (Henderson, 1990), for which the diffraction pattern is predicted to be halved, has been calculated for apoferritin crystals with different metal ion concentrations. It was found that the presence of transition metal ions reduced the time to reach the Henderson limit by a factor of two in the case of 0.5 M $FeCl_2$ at an X-ray energy of 13.2 keV (0.94 Å) (Murray & Garman, 2002). Thus metal-containing radioprotectants would have to be highly effective to outweigh the deleterious effect caused by the increased absorption cross section. We have thus selected radioprotectants which do not contain highly absorbing (metal) atoms. The toxicity of the compounds must also be considered, as hazardous compounds are less convenient for common use.

This paper reports the systematic screening, by monitoring the optical absorption spectra of cryocooled solutions when irradiated with X-rays, of a wide range of putative radio-protectants for potential use in macromolecular crystallography.

2. Disulfide/thiol test systems

Cysteine (SH) (Fig. 1a) and cystine (SS) (Fig. 1b) were chosen to model the thiol groups and disulfide groups, respectively, of proteins. The latter is a known victim of radical attack on protein molecules at room temperature (Favaudon et al., 1990) and, as mentioned above, also at 100 K. A cyclic peptide such as oxidized α-lipoic acid (Fig. 1c) may also provide an appropriate model system for protein disulfide bonds, as the recombination probability of the two sulfur radicals produced by S—S bond breakage is higher, thus mimicking more closely an intramolecular disulfide bond in a protein (Murray, 2004). Reduced α-lipoic acid (Fig. 1d) and reduced dithiothreitol (DTT) (Fig. 1e) are two additional possible models for thiol systems. In pulse radiolysis experiments, it has been found that 1,3- and 1,4-disulfhydryl-containing molecules showed particular stability of their disulfide radicals towards dissociation into $RS^- + RS^\bullet$ (the sulfhydryl group is a sulfur atom bonded to a hydrogen atom) (Armstrong, 1990). For oxidized α-lipoic acid, where the sulfhydryls are separated by three carbon atoms, the possibility of formation of a five-membered ring would stabilize the protonated disulfide radical. The ability to form cyclic structures also leads to enhanced stability in disulfide anions. Thus the lipoate anion radical at high pH appears to be stable to dissociation (i.e. ring opening), while linear disulfide anions and other monothiols decompose into $RS^- + RS^\bullet$. The absorption spectra of cyclic disulfide radical anions are subject to large variations in both the position of the maximum absorption wavelengths and the value of the molar extinction coefficients. The deprotonated and protonated forms of the disulfide anion of oxidized α-lipoic acid have absorption spectrum peaks at 420 nm and 380 nm and ε_{max} values of 9000 and 6000 M^{-1} cm^{-1}, respectively (Armstrong, 1990).
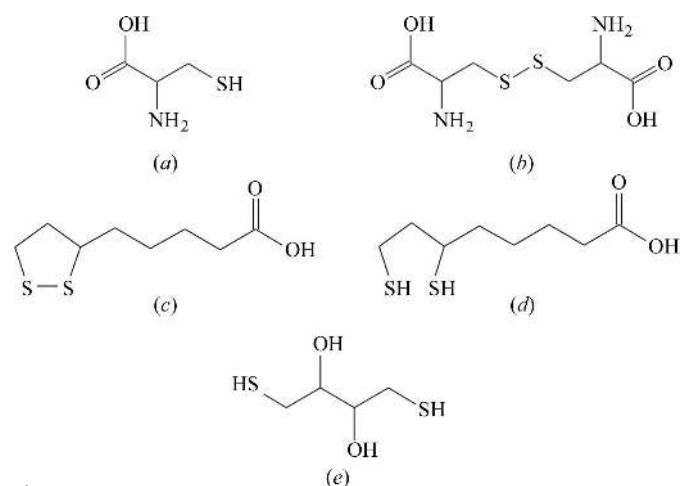

Figure 1
Model disulfide/thiol systems: (a) cysteine, (b) cystine (c) oxidized α-lipoic acid, (d) reduced α-lipoic acid and (e) reduced DTT.

Upon capture of an electron, disulfide bonds form disulfide radical anions, $RSSR^{\bullet-}$, which can undergo spontaneous and reversible bond rupture (Armstrong, 1990; Favaudon et al., 1990). Protonation of this radical leads to the formation of the disulfide radical $RSSRH^{\bullet}$, with a concomitant shift of the equilibrium towards the broken state (Armstrong, 1990). Upon rupture, a thiol, RSH, and a thiyl, $RS^{\bullet}$, radical are formed, with the absorbance of the thiyl radical $RS^{\bullet}$ having a maximum near to 340 nm and being much weaker than that of the disulfide radical anion (Armstrong, 1990).

The suitability of oxidized α-lipoic acid and reduced DTT as models for protein disulfide bonds in the bonded and unbonded states was investigated. For our experiments, alkaline conditions were favoured over acidic conditions in the sample preparation because, firstly, the radical anions of oxidized α-lipoic acid are expected to be more stable at higher pH and, secondly, acidic solutions buffered with HCl always show a peak at 340 nm. The chloride ion Cl^- can react with the radiolytic products of water to produce species such as $Cl_2^{\bullet-}$, as shown below, giving a signal at 340 nm in acidic solution (Neta et al., 1988):

$$Cl^- + {}^{\bullet}OH \longleftrightarrow ClOH + Cl^- \longleftrightarrow Cl_2^{\bullet-} + OH^-.$$
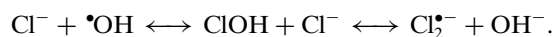
Pulse radiolysis experiments have revealed that the disulfide radical anion and its protonated form absorb with maxima at 425–440 nm and 400 nm, respectively (Favaudon et al., 1990; Armstrong, 1990). In a study by Weik et al. (2002), the observed maximum at 400 nm in the absorption spectrum from X-ray-exposed native Torpedo californica acetylcholinesterase crystals was identified as being from a disulfide radical anion species.

To observe the production of this radical we have monitored the absorbance between 270 nm and 800 nm of cryocooled liquid samples while irradiating them with an X-ray beam, by means of an online microspectrophotometer installed at the European Synchrotron Radiation Facility (ESRF). To test putative radioprotectants, the presence or absence of the 400 nm disulfide radical anion peak was taken as the measure of the effectiveness of the radioprotectant reagent. For example, a peak at 400 nm on a sample containing 30% ethylene glycol (EG) + 0.1 M cystine (SS) + 0.5 M radioprotectant indicated that radiation damage had affected the disulfide bond, and that the radioprotectant had failed to protect it. However, if the peak was absent then we suggest that the radioprotectant has been effective and may therefore be useful in preventing damage in protein crystals.

3. Materials and methods

3.1. Sample preparation

Samples were prepared as a mixture of a disulfide or thiol compound with radioprotectant and appropriate cryoprotectant. The bonded (cystine, or oxidized α-lipoic acid; modelling the disulfide groups) or unbonded (cysteine, or reduced DTT; modelling the thiol groups) sulfur compounds were at a concentration of 0.1 M. The radioprotectant concentration varied between 0.1 M and 0.5 M. The highest concentration was tried first and, if the radioprotectant had any effect, lower concentrations than this were tried to attempt to establish a minimum effective concentration. If there was any uncertainty as to the result of the radioprotectant tested at 0.5 M, the concentration was increased to 1.0 M and the experiment repeated. For the α-lipoic acid test system, the optical signal was smaller in magnitude than that for cystine, so only the cystine was used for establishing the minimum effective scavenger concentration.

The cryoprotectant agent concentration was 30% v/v (5.38 M) in all cases; mainly EG was used, but glucose and glycerol were also tested to ensure that the choice of agent did not affect the appearance or otherwise of the disulfide radical anion peak (see 'Controls' in Table 1). Precipitates formed in some of the initial mixtures, so, in order to dissolve them, 5 M NaOH was added to the 1 ml final sample volumes. It was added 50 μl at a time, with each addition separated by 20 s of vigorous mixing on a vortex machine, until there was no precipitant remaining. The pHs of all solutions (see Table 1) were measured using a calibrated Schott CG840 pH meter.

3.2. Cryocooling of samples

Liquid samples were held by surface tension in 0.5 mm-diameter 20 μm-thick rayon cryoloops (Molecular Dimensions). Films were extracted by dipping the loop into the sample and smoothly extracting it with its plane perpendicular to the liquid surface. This minimizes the thickness of the film in the loop and leads to lower optical absorption and lower background than when thicker films are used. The liquid films were flash-cooled straight into a 100 K nitrogen stream provided by an Oxford Cryosystems 600 (or 700) series cryostream. If ice formation occurred rather than the desired amorphous glass, the spectra were uninterpretable due to the high light scattering of ice.

3.3. X-ray source and microspectrophotometer

Data were collected at 100 K on the undulator beamlines ID14-EH2 (0.939 Å) and ID14-EH4 (0.979 Å) at the ESRF in Grenoble, France. The optical spectra were recorded using an online Ocean Optics HR2000 microspectrophotometer (Fig. 2), and full details of the experimental arrangement can be found in Ravelli et al. (2007). The microspectrophotometer was used to monitor the presence of the disulfide radical anion $RSSR^{\bullet-}$ generated during X-ray exposure in the sample under mostly alkaline conditions. The light sources available were either a DH2000 deuterium or tungsten halogen lamp, or both in combination. The latter was used for sample alignment and the former to record the absorption spectra. The light was delivered to the top lens through a 100 μm 2UV-SR fibre optic and collected from the bottom lens using a 600 μm fibre optic. Together with the HR2000 CCD detector in the microspectrophotometer, this allowed optical absorption spectra to be collected between 270 nm and 800 nm. Optical spectra were recorded every 120 ms throughout the experiment, starting a few seconds before the sample was exposed to

Table 1
The results of the scavenger screening experiments.

* = 5 *M* NaOH added in μl to 1 ml sample volume. EG = ethylene glycol. Glyc = glycerol. Gluc = glucose. SC = scavenger concentration (*M*). OP = other peaks. BHT = butylated hydroxy toluene.

Test system 0.1 *M*	Cryoprotectant	Scavenger	SC	400nm	600nm	OP	*	pH
Controls								
–	EG 30%	–	–	–	–	550	–	5.65
Cystine	EG 30%	–	–	Yes	–	–	100	12.53
Cysteine	EG 30%	–	–	–	–	–	–	4.7
Reduced DTT	EG 30%	–	–	–	Yes	–	–	3.20
α-Lipoic acid	EG 30%	–	–	Yes	–	–	50	12.49
–	Gluc 30%	–	–	–	–	–	–	3.69
Cystine	Gluc 30%	–	–	Yes	–	–	100	10.08
Cysteine	Gluc 30%	–	–	–	–	–	–	3.55
Cystine	Glyc 44%	–	–	Yes	–	–	50	12.10
Cysteine	Glyc 44%	–	–	–	–	–	–	3.68
NaOH 5 *M*	–	–	–	–	Yes	–	n/a	13.70
Samples								
–	EG 30%	Ascorbate	0.5			360		7.66
Cystine	EG 30%	Ascorbate	1.0	–	–	380	150	11.68
Cystine	EG 30%	Ascorbate	0.5	–	–	350	50	11.55
Cystine	EG 30%	Ascorbate	0.4	–	–	350	–	6.4
Cystine	EG 30%	Ascorbate	0.3	–	–	–	150	12.9
Cystine	EG 30%	Ascorbate	0.2	Yes	–	–	150	13.12
Cystine	EG 30%	Ascorbate	0.1	Yes	–	–	100	13.18
Reduced DTT	EG 30%	Ascorbate	0.5	–	–	350	–	6.17
α-Lipoic acid	EG 30%	Ascorbate	0.5	–	–	380	50	10.04
–	EG 30%	Quinone	0.5	–	–	410	–	3.3
Cystine	EG 30%	Quinone	1.0	–	–	–	150	12.82
Cystine	EG 30%	Quinone	0.5	–	–	–	150	12.35
Cystine	EG 30%	Quinone	0.4	–	–	–	150	13.3
Cystine	EG 30%	Quinone	0.3	Yes	–	–	150	13.3
Cystine	EG 30%	Quinone	0.2	–	–	–	150	12.95
Cystine	EG 30%	Quinone	0.1	Yes	–	–	150	13.26
α-Lipoic acid	EG 30%	Quinone	0.5	–	–	380	50	11.30
–	EG 30%	TEMP	0.5	–	–	–	–	4.25
Cystine	EG 30%	TEMP	0.5	Yes	–	–	200	12.37
Cystine	EG 30%	TEMP	0.3	Yes	–	–	100	13.09
Cystine	EG 30%	TEMP	0.1	Yes	–	–	100	13.27
α-Lipoic acid	EG 30%	TEMP	1.0	–	–	–	150	8.48
α-Lipoic acid	EG 30%	TEMP	0.5	–	–	330	100	8.12
Cystine	Glyc 30%	Glucose	1.0	Yes	–	–	50	12.15
Cystine	Glyc 30%	Maltose	1.0	Yes	–	–	50	8.01
Cystine	Glyc 30%	Maltotriose	1.0	Yes	–	–	50	8.17
Cystine	Glyc 30%	Trehalose	1.0	Yes	–	–	50	12.10
Cystine	Glyc 30%	Sucrose	1.0	Yes	–	–	50	11.57
Cystine	EG 30%	Sucrose	0.5	Yes	–	–	100	8.97
α-Lipoic acid	EG 30%	Sucrose	0.5	Yes	–	330	50	11.57
Cystine	EG 30%	SH (cysteine)	0.5	Yes	–	–	100	12.71
Cystine	EG 30%	BHT	0.5	Yes	–	–	100	13.01
Cystine	EG 30%	Glutathione	0.5	Yes	–	–	100	9.69
Cystine	EG 30%	Methacrylate	0.5	Yes	–	–	100	7.69
Cystine	EG 30%	Thiourea	0.5	Yes	–	–	50	10.87
Cystine	EG 30%	TRIS	0.5	Yes	–	–	50	10.35
α-Lipoic acid	EG 30%	TRIS	0.5	Yes	–	330	–	6.77
Cystine	EG 30%	HEPES	0.5	Yes	–	570	100	9.66
α-Lipoic acid	EG 30%	HEPES	0.5	Yes	–	330	100	7.87
Cystine	EG 30%	*t*-Butanol	0.5	Yes	–	–	100	12.56
Cystine	EG 30%	Ethanol	0.5	Yes	–	570	100	12.48
Cystine	EG 30%	Ethanol	0.5	Yes	–	–	100	12.96
Cystine	EG 30%	Acetone	0.5	Yes	–	–	100	13.20
Cystine	Glyc 30%	PEG 4000	12%	Yes	Yes	–	150	13.59
Cystine	EG 30%	PEG 4000	20%	Yes	–	–	150	13.70
Cystine	Glyc 30%	PEG 4000	45%	Yes	–	–	150	13.70
–	EG 30%	Reduced DTT	0.5	–	–	380	–	7.4
Cystine	EG 30%	Reduced DTT	0.5	–	–	380	100	9.50
α-Lipoic acid	EG 30%	Reduced DTT	0.5	–	–	380	100	10.00

X-rays in a regime of either 10×1 s or 20×1 s, each exposure to the X-ray beam being separated by a 5–8 s 'beam off' period (detector readout time during which optical spectra were still recorded). Prior to any X-ray irradiation, rotation of the sample through $360°$ in φ while monitoring the absorption spectrum was necessary, in order to find the sample position with the best optical peak absorption to background ratio. Several repeat experiments were carried out on each sample to check reproducibility.

4. Results

The results of the radioprotectant screening experiments are compiled in Table 1. Figs. 3, 4 and 5 show different views of the absorption peaks observed from various samples. The graph colours are related to the magnitude of the absorption, with blue being the lowest and red being the highest. They are plotted on a relative rather than an absolute scale. In each case the left-hand graph (i) shows optical absorption (*y* axis) *versus* wavelength in nm (*x* axis). They are selected at the point in time where the exposure reached its highest value. The central graphs (ii) are plots of wavelength in nm (*y* axis) *versus* time in s (*x* axis) and allow all recorded peaks to be simultaneously observed. The right-hand graphs (iii) (where present) are plots of absorption (*y* axis) *versus* time in s (*x* axis) selected at the peak wavelength from (ii), and display a sawtooth-like pattern as the shutter on the beamline is opened and closed, before finally remaining closed. This alternating exposure and blocking of the X-ray beam causes a peak in absorption, which saturates after only a few 1 s exposures, and decays exponentially with time upon shutter closure. An absorption peak around 600 nm has been identified as being due to the solvated electron e^{-}_{aq} (Gould, 1968), and the origins of the other peaks we were able to identify are listed in Table 2.

The spectra displayed throughout this paper are difference spectra, produced by recording both a reference spectrum prior to X-ray irradiation and an absorption spectrum during sample irra-
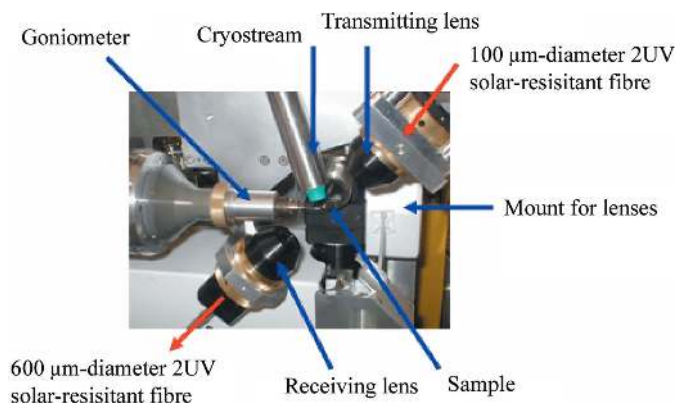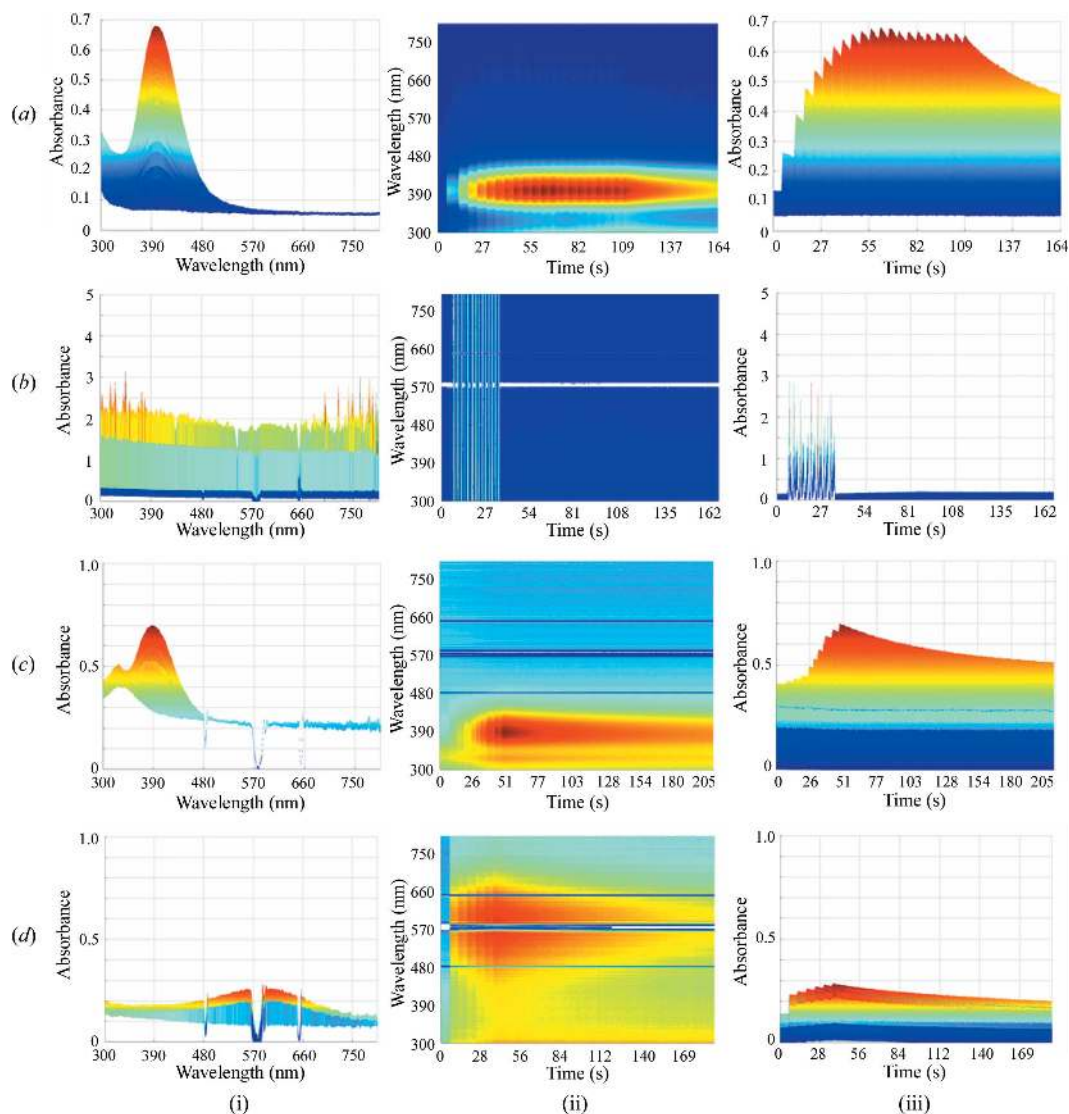
Figure 2
Experimental arrangement showing microspectrophotometer lenses, sample and cryostream. All of these must to be centred on the X-ray beam position on the sample.

diation. The absorption plots shown in Figs. 3–5 represent the difference between the two spectra in each case. The troughs seen at 492 nm, 587 nm and 661 nm in the spectra [*e.g.* in Figs. 3*c*(i) or 3*d*(i)] were due to the saturation of the counts in the photodetector from the deuterium lamp used to collect the reference spectrum. The high intensity of the deuterium lamp at these three wavelengths relative to the rest of the spectrum causes the absorption of the samples to be greatly under-estimated at these values.

4.1. Disulfide/thiol test systems

The plot in Fig. 3*a*(i) (30% EG + 0.1 *M* cystine) displays a clear strong absorption peak at 400 nm characteristic of the disulfide radical anion. The 400 nm peak is not due to EG, as seen in Table 1, where it is present with EG and cystine (Table 1, line 2), but absent with EG only (Table 1, line 1). The

Figure 3
The graph colours are related to the magnitude of absorption, with blue being the lowest and red being the highest. (*a*) EG/SS. (i) Peak at 400 nm corresponding to disulfide radical anion. (ii) Aerial view showing single peak present at 400 nm. (iii) Decay plot with time of the 400 nm peak. (*b*) EG/SH. (i) No peak present at 400 nm. (ii) Aerial view showing featureless spectra. (iii) No decay plot produced. (*c*) EG/oxidized *α*-lipoic acid. (i) Produces 400 nm peak and small peak around 330 nm. (ii) Both peaks are visible in spectrum. (iii) Decay plot. (*d*) EG/reduced DTT. (i) Reduced DTT did not produce a peak at 400 nm but has small peak at 600 nm. (ii) 600 nm peak visible. (iii) Decay plot.

400 nm peak is the only peak in the spectrum, as seen in Fig. 3a(ii). The sawtooth pattern in Fig. 3a(iii), which saturates after the first nine or ten pulses, is produced from alternately opening and closing the shutter. The X-ray beam induces the radicals seen as peaks which decay as the radical species are first populated and then recombine.

The graphs in Fig. 3(b) show the results from the thiol (0.1 M cysteine) test system. Here, since there is no disulfide bond, no disulfide radical anion is present and hence there is no peak at 400 nm [Fig. 3b(i)]. Fig. 3b(ii) shows the full spectrum of wavelengths scanned and there are clearly no peaks present, in turn giving a featureless time decay plot, as seen in Fig. 3b(iii).

The results from 0.1 M oxidized α-lipoic acid in Fig. 3c(i) indicate that it is also a suitable test system to model the disulfide bonds of proteins, as it produces the characteristic disulfide radical anion at 400 nm. It also has another smaller peak around 330 nm which we have not been able to identify. The large 400 nm peak dominates Fig. 3c(ii), and the sawtooth pattern induced by the X-ray irradiation regime can be seen in the time plot [Fig. 3c(iii)].

As expected, the 0.1 M reduced DTT did not produce a disulfide radical anion peak at 400 nm. It did however produce a small peak at 600 nm [Fig. 3d(i)], corresponding to absorption by e_{aq}^{-}.

Figure 4
(a) EG/SS/0.5 M ascorbate. (i) Peak at 360 nm. (ii) No peak present at 400 nm. (b) EG/SS/0.2 M ascorbate. (i) Lower concentration of ascorbate shows small peak around 400 nm. (ii) No peaks in spectrum at 400 nm. (c) EG/SS/0.5 M quinone. (i) Quinone seems to still quench 400 nm peak at 0.5 M. (ii) No peak at 400 nm.

4.2. Ascorbate as a radical radioprotectant

Ascorbate was shown to be an effective radical radio-protectant for both the cystine and oxidized α-lipoic acid test systems. As can be seen from Table 1, the effectiveness of the ascorbate decreased as its concentration was reduced. Although its effectiveness probably increases at the higher concentrations, no large differences in scavenging ability were visible between 1 M and 0.3 M where the 400 nm peak was quenched. Below 0.3 M the scavenging ability started to diminish and the characteristic 400 nm peak of the disulfide radical anion started to appear. This is nicely illustrated in Fig. 4a(i) where the ascorbate completely quenches the 400 nm peak of the 30% EG/0.1 M cystine/0.5 M ascorbate sample. There is a peak at 360 nm due to the ascorbate radical (observed in the 30% EG + 0.5 M ascorbate control sample) but, as can be seen in Fig. 4a(ii), there is clearly no peak at 400 nm. The lower concentration of ascorbate in the 30%
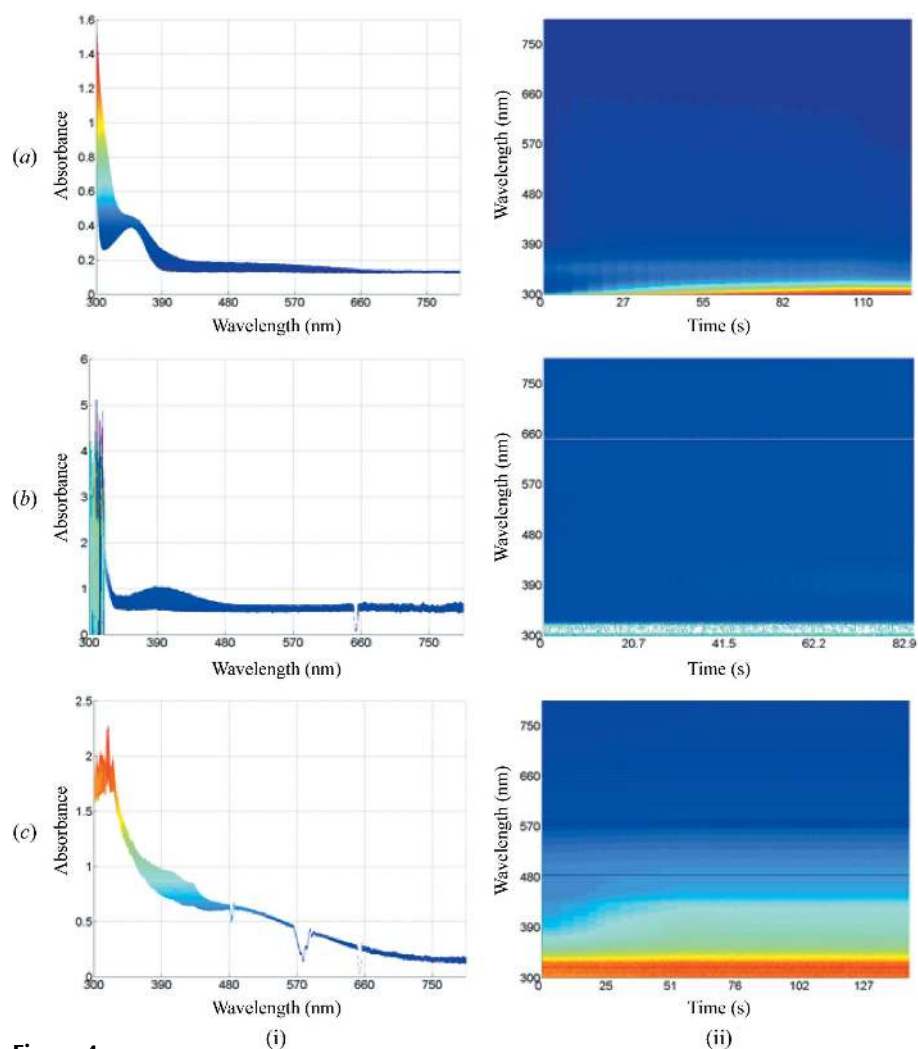
Table 2
Values of absorption peak maximums of the species present in the samples tested.

Source	Peak (nm)
Ascorbate	350–380
α-Lipoic acid	330, 390–400
Quinone	330, 400
Disulfide radical anion	400
Solvated e^{-}	590–600

ethylene glycol/0.1 M cystine/0.2 M ascorbate sample can be seen to give a reduced scavenging capacity with a small peak appearing at 400 nm in Fig. 4b(i), but it is quenched compared with the prominent peak at 400 nm in the sample without the ascorbate added [Fig. 3a(i)]. As the concentration of ascorbate tested was reduced further, the peak at 400 nm reappeared, indicating the failure of the ascorbate at 0.1 M to prevent the formation of the disulfide radical anion (Table 1).

4.3. Quinone as a radical radioprotectant

Quinone (1,4-benzoquinone) also appears to be an effective radioprotectant on both the cystine and oxidized α-lipoic acid test systems, scavenging well from 1 M down to 0.4 M in the case of cystine, and at 0.5 M for oxidized α-lipoic acid (Table 1). At quinone concentrations lower than 0.4 M the disulfide radical anion peak appears at 400 nm indicating that at this concentration the radioprotectant is ineffective. Figs. 4c(i) and 4c(ii) show the 30% EG/0.1 M cystine/0.5 M quinone sample, where quinone scavenging is clearly effective. For the control EG and 0.5 M quinone sample, a small peak was observed just above 400 nm which was due to the quinone radical, known to absorb at 424 nm (von Sonntag *et al.*, 2004). This peak was sharper than that of the disulfide radical anion and much smaller in magnitude.

4.4. TEMP as a radical radioprotectant

TEMP (2,2,6,6-tetramethyl-4-piperidone) was effective on the oxidized α-lipoic acid test system, but then unexpectedly not on the cystine test system (Table 1). In Figs. 5a(i) and 5a(ii), for the 30% EG/0.1 M oxidized α-lipoic acid/0.5 M TEMP, the peak at 400 nm from oxidized α-lipoic acid was not present, showing that the radioprotectant is effective. However, at 0.5 M and below in the corresponding cystine test system, there was a clear peak at 400 nm. This was the only example of a radioprotectant that gave qualitatively differing scavenging results on the two disulfide test systems. The reason for this is as yet unknown.
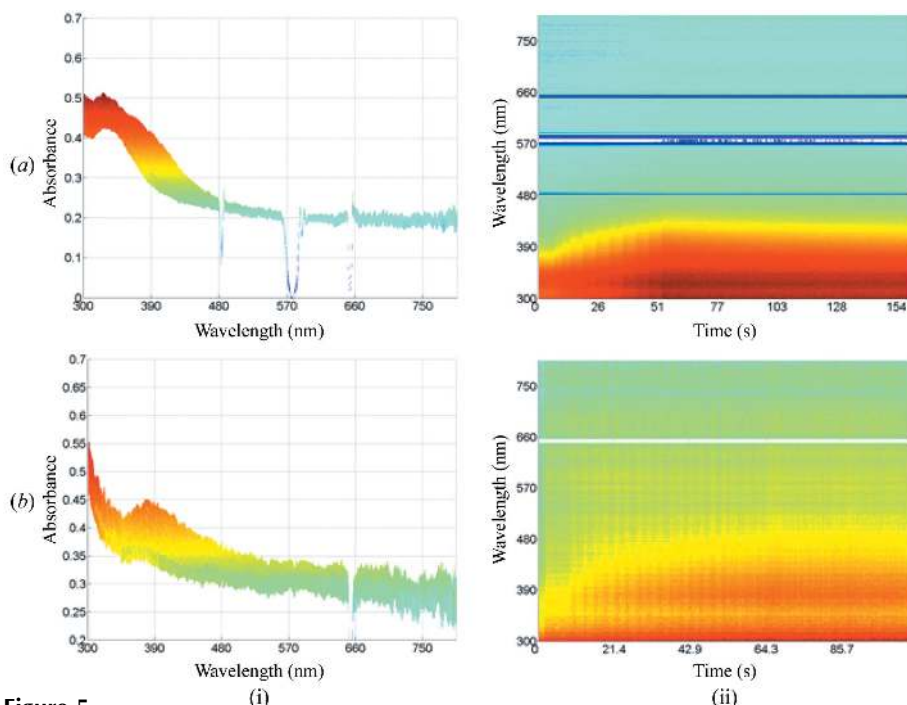
4.5. DTT as a radical radioprotectant

Reduced DTT seemed to show radioprotective effectiveness on the two model disulfide systems, as displayed for the 30% EG/0.1 M cystine/0.5 M DTT sample, shown in Figs. 5b(i) and 5b(ii). There are signs of a small peak at 380 nm from the reduced DTT (see Table 1), which is close to where the test system peak is expected (400 nm). However, the peak is substantially reduced in magnitude and slightly reduced in wavelength compared with the strong 400 nm peak from cystine seen in Fig. 3a(i), which had no radioprotectant added. We note that reduced DTT is an H-atom donor under acidic conditions and an electron donor under alkaline conditions, implying that the radioprotective capacity will vary with pH.

4.6. Other radioprotectants

The other putative radioprotectants investigated and listed in Table 1 which failed to provide scavenging capability included the sugars, glucose, maltose, maltotriose, trehalose and sucrose at 1 M concentration; PEG 4 K at 12%, 20% and 45%; the thiol cysteine; butylated hydroxyl toluene; glutathione; methacrylate; thiourea; TRIS (hydroxymethyl aminoethane); HEPES (N-2-hydroxyethylpiperazine-N'-2-ethane-sulfonic acid); *t*-butanol; ethanol and acetone, all at 0.5 M.

Contrary to the results of Cascio *et al.* (1984) on PEG as a scavenger at room temperature, we observed no positive effects of PEG as a radioprotectant. However, the cryoprotectants themselves may well be affecting the progression of radiation damage, but this is difficult to investigate since cryoprotectants are required to form an amorphous glass. Thus this issue is still to be addressed.

We note that, although acetone is known to be a very effective electron scavenger, it seems unable to quench the disulfide radical anion.
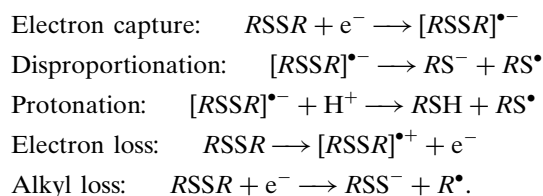
4.7. Summary

Upon irradiation, the model disulfide systems selected produced strong 400 nm peaks for cystine and oxidized α-lipoic acid. As expected, the 400 nm peak was absent in the thiol model systems of cysteine and reduced DTT. In the case of reduced DTT there was a peak at 600 nm assigned to solvated electrons. Ascorbate quenched the 400 nm peaks of both cystine and oxidized α-lipoic acid, and seems to be an effective radioprotectant for concentrations ranging from 1 M down to 0.3 M. At 0.2 M ascorbate concentration, the 400 nm peak started to reappear. Quinone was also effective on cystine and oxidized α-lipoic acid. It lost its scavenging capacity on the cystine test system at around 0.3 M concentra-

Figure 5
(*a*) EG/oxidized α-lipoic/0.5 M TEMP. (i) Peak around 340 nm. (ii) No peak at 400 nm. (*b*) EG/SS/ reduced 0.5 M DTT. (i) Small peak at 400 nm. (ii) Peaks at 300 nm and 380 nm.

tion. TEMP was only effective on oxidized α-lipoic acid and not on cystine. Reduced DTT, when tested as a radical radioprotectant, was effective in eliminating the peak of cystine and oxidized α-lipoic acid at 400 nm.

5. Discussion

Disulfide bonds have previously been found to be the most radiation-damage-sensitive sites in proteins, and so the screening of putative radical radioprotectants has been undertaken by monitoring the optical absorption of the disulfide radical anion. From the experiments, the two most successful of the radioprotectants tested appear to be ascorbate and quinone. The mechanism of their protective effect probably comes either from the ability of a radioprotectant molecule to donate an electron, thus allowing the formation of spin-paired electrons at locations that would otherwise be unstable radical species and itself becoming a stable radical (ascorbate), or from the ability of the radioprotectant to react with the mobile electrons and form relatively stable products (quinone).

The possible mechanisms of disulfide bond breakage include (Prutz *et al.*, 1989):

Electron capture: $RSSR + e^- \longrightarrow [RSSR]^{\bullet-}$

Disproportionation: $[RSSR]^{\bullet-} \longrightarrow RS^- + RS^{\bullet}$

Protonation: $[RSSR]^{\bullet-} + H^+ \longrightarrow RSH + RS^{\bullet}$

Electron loss: $RSSR \longrightarrow [RSSR]^{\bullet+} + e^-$

Alkyl loss: $RSSR + e^- \longrightarrow RSS^- + R^{\bullet}$.

The ejected electrons in proteins readily migrate along the protein backbone by tunnelling through the CH(R) groups to the next large π^* orbitals even at 100 K, illustrated in Fig. 6(a) (Symons, 1999). The electron-rich carbonyl group then exists with a single unpaired electron in a previously unoccupied π^* orbital (Figs. 6b and 6c), until they reach an electron-affinic group such as the disulfide bond. The disulfide radical anions then have an electron in a σ^* orbital which is a highly unstable anti-bonding molecular orbital and is the reason that it is particularly susceptible to partial reduction and cleavage. The S—S bond in the radical anion is known as a two-centre three-electron bond (2c-3e), and the S—S bond length is longer for the anion than for the neutral parent (Berges *et al.*, 2006).

If disulfide bonds, which are known to be a location of electron reactions in protein chains, are unable to trap any electrons because the electrons are quenched by radioprotectant molecules, then the potential for radiation-damage protection exists. Fig. 7 shows the chemical structure of the radioprotectants that displayed the most promising results; they were able to quench the 400 nm peak characteristic of the disulfide radical anion.

The pH of the system is likely to be an important parameter governing the relevant radiation chemistry. Ascorbic acid has a pK_a value of 4.1 and under physiological conditions it is largely dissociated, forming the monovalent ascorbate anion. It has been established as a major water-soluble intracellular antioxidant (Asmus *et al.*, 1996). Ascorbate (at 193 K) can
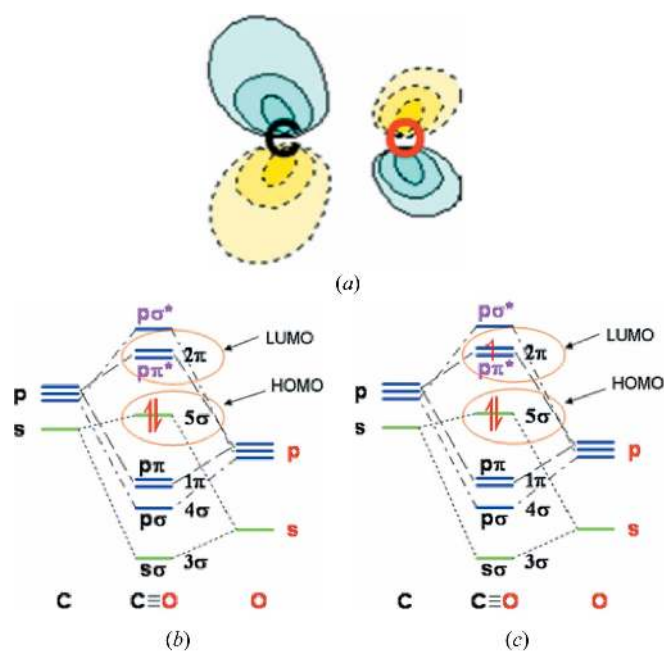

Figure 6
(*a*) Lobes of antibonding π^* orbitals between which mobile electrons can migrate at 100 K. (*b*) Molecular orbital diagram showing the HOMO (highest-occupied molecular orbital) in a stable carbonyl group and the LUMO (lowest-unoccupied molecular orbital) through which the electrons are transported when mobile electrons are present. (*c*) LUMO occupied by mobile electron.
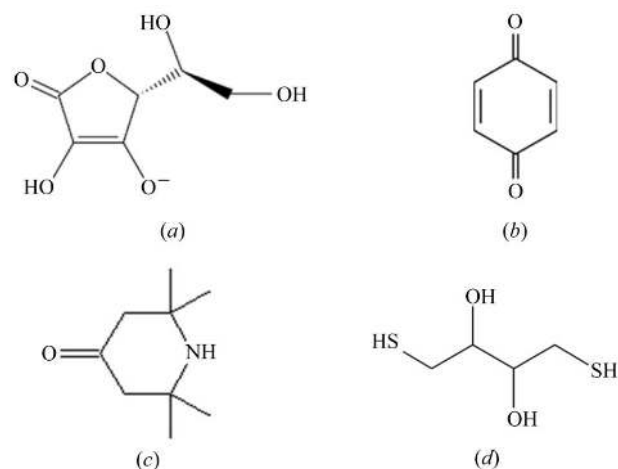

Figure 7
The most promising molecules from the wide number of potential scavengers tested. (*a*) Ascorbate. (*b*) Quinone. (*c*) TEMP. (*d*) Reduced DTT.

readily repair all oxidizing free radicals with greater reduction potentials, which includes hydroxyl radicals (Zbikowska *et al.*, 2006). Because the ascorbyl radical has its unpaired electron in a highly delocalized π system, it is a relatively unreactive free radical. This is likely to be the basis for successful scavenging in protein crystals at all temperatures. The ability to delocalize the radical over multiple sites within an ascorbate molecule will increase the overall stability of the radical molecule. For quinone, it is known that semiquinone free radicals are markedly stabilized at alkaline pH, thus furthering the case for using a high pH (Swartz & Swartz, 1983). High pH was
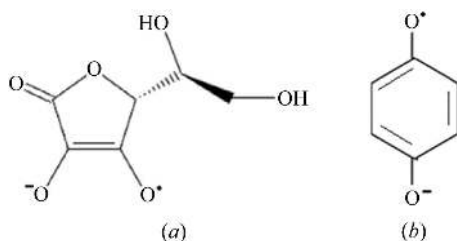
Figure 8
The likely radical anions formed by (*a*) ascorbate and (*b*) quinone. The radical is delocalized over the three oxygen atoms attached to the ring of the ascorbate radical, and from one oxygen atom across the ring to the other oxygen for the quinone radical.

necessary in most of our samples in order to dissolve the disulfide modelling compounds. Naturally occurring quinones or quinone-like substances include vitamin K, vitamin E, ubiquinone, plastoquinone, vitamin C (ascorbate) and melanin, many of which are recognized radioprotectants at physiological temperatures.

The fundamental equation of free-radical repair is

$$RSH + A^{\bullet} \longleftrightarrow RS^{\bullet} + AH$$
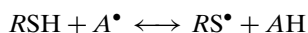
where $A^{\bullet}$ is an acceptor radical (Armstrong, 1990). The ascorbate radical (Fig. 8*a*) can delocalize the radical over the three carbonyl oxygen sites and the quinone (Fig. 8*b*) can delocalize the radical from the oxygen atom on one side of its ring to the oxygen atom on the other side of the ring. The method of scavenging by TEMP and reduced DTT is less clear, but they are known electron scavengers. Perhaps the N atom can donate an electron and the resultant TEMP radical be stabilized by the electron-inductive effects of the adjacent alkyl groups. TEMP appeared effective as a radioprotectant on only oxidized α-lipoic acid, and the results for the scavenging capacity of reduced DTT suggest that it might have some radioprotective potential.

The radioprotectants selected for study and presented in this paper were selected from a long list of potential radio-protectants suggested in the literature covering widely differing scientific fields. Their usefulness in macromolecular protein crystallography is as yet unknown in the majority of cases. They were chosen on the basis that they showed good free-radical scavenging ability in other applications and because they lacked any highly absorbing atoms such as transition metals. As can be seen from Table 1, many of the putative radioprotectants tested did not quench the 400 nm peak characteristic of the disulfide radical anion. The sugars were found to be ineffective as radioprotectants in our experiments, a result which supports a previous study by Betts (2004), who examined electron density maps of influenza virus N9 neuraminidase crystals with and without glucose added as a radioprotectant, and found glucose to be completely ineffective in quenching damage.

We note that the method we employed for testing useful radioprotectants may not give positive results for a radioprotectant that would protect a protein crystal from radiation damage at locations other than the disulfide bonds (*e.g.* from decarboxylation of glutamates and aspartates) (Kauffmann *et*

al., 2006). The concentrations of cryoprotectant agents chosen for this study were within the range commonly used in macromolecular cryocrystallography and similar to those used in previous work on screening radioprotectants for protein crystals (Murray & Garman, 2002; Betts, 2004; Kauffmann *et al.*, 2006). This was to ensure that the results would have relevance for real-life cases. The microspectrophotometer has allowed the testing of a large number of candidate radio-protectants, and protective effects towards the disulfide species are particularly helpful as these are the sites of greatest susceptibility to radiation damage. However, all the suggested radioprotectants require testing on protein crystals, and detailed analysis of electron density maps to confirm their utility for macromolecular crystallography.

As well as testing the effectiveness of the radical radioprotectants, it had been hoped that the microspectrophotometer could also be used as an online metric for radiation damage by detecting characteristic radical species formed during exposure to X-rays on the beamline (Murray, 2004). However, it was seen that the absorption maxima appeared rapidly and saturated usually within the first few 1 s exposures, before decaying away exponentially. Thus monitoring the appearance of the 400 nm absorption peak by using the online microspectrophotometer (to measure the extent of radiation damage) is unlikely to be a generally applicable online radiation-damage metric in MX, since it occurs on time scales much shorter than the fading of the X-ray diffraction patterns.

6. Conclusions

The evidence for the potential utility of ascorbate as a radical radioprotectant in protein crystallography has been re-inforced. New radioprotectants have also been identified, the most promising of which appears to be quinone, but additional candidates for further investigation are TEMP and reduced DTT.

The other putative radioprotectants investigated which failed to provide quenching of disulfide radical production included the sugars, glucose, maltose, maltotriose, trehalose and sucrose at 1 *M* concentration; PEG 4 K at 12%, 20% and 45%; the thiol cysteine; butylated hydroxyl toluene; gluta-thione; methacrylate; thiourea; TRIS; HEPES; *t*-butanol; ethanol and acetone, all at 0.5 *M*.

This study has also shown that both the cystine and oxidized α-lipoic acid seem to be suitable models for disulfide bonds in proteins, giving a clear peak at 400 nm on S—S bond breakage. As anticipated, the cysteine and reduced DTT systems did not produce this peak.

Further work will include testing the potential radical radioprotectants identified by the experiments described above on protein crystals, and examining the data statistics and quality of electron density maps in the presence and absence of these radioprotectants. A study of the effects of the pH on their scavenging capacity is also necessary. The microspectrophotometer will continue to serve as a useful

diagnostic tool for identifying new candidates to use as radioprotectants.

References

Armstrong, D. A. (1990). *Sulfur-Centered Reactive Intermediates in Chemistry and Biology*, pp. 121–134. New York: Plenum.

Asmus, K. D., Bensasson R. V., Bernier, J. L., Houssin, R. & Lands, E. J. (1996). *Biochem. J.* **315**, 625–629.

Berges, J., Fuster, F., Jacquot, J. P., Silvi, B. & Houee-Levin, C. (2000). *Nukleonika*, **45**, 23–29.

Berges, J., Rickards, G., Rauk, A. & Houee-Levin, C. (2006). *Chem. Phys. Lett.* **421**, 63–67.

Betts, S. (2004). Part II project. Oxford University, UK.

Burmeister, W. P. (2000). *Acta Cryst.* D**56**, 328–341.

Cascio, D., Williams, R. & McPherson, A. (1984). *J. Appl. Cryst.* **17**, 209–210.

Dick, L. A., Malfant, I., Kuila, D., Nebolsky, S., Nocek, J. M., Hoffman, B. M. & Ratner, M. A. (1998). *J. Am. Chem. Soc.* **120**, 11401–11407.

Favaudon, V., Tourbez, H., Houée-Levin, C. & Lhoste, J.-M. (1990). *Biochemistry*, **29**, 10978–10989.

Fischer, M. & Devlin, J. P. (1995). *J. Phys. Chem.* **99**, 11584–11590.

Fulford, J., Nikjoo, H., Goodhead, D. T. & O'Neill, P. (2001). *Int. J. Radiat. Biol.* **77**, 1053–1066.

Garman, E. (1999). *Acta Cryst.* D**55**, 1641–1653.

Garman, E. (2003). *Curr. Opin. Struct. Biol.* **13**, 545–551.

Garman, E. F. & Schneider, T. R. (1997). *J. Appl. Cryst.* **30**, 211–237.

George, G. N., Hedman, B. & Hodgson, K. O. (1998). *Nature Struct. Biol., Synchrotron Suppl. (August)*, pp. 645–647.

George, S. D. B., Basumallick, L., Szilagyi, R. K., Randall, D. W., Hill, M. G., Nersissian, A. M., Valentine, J. S., Hedman, B., Hodgson, K. O. & Solomon, E. I. (2003). *J. Am. Chem. Soc.* **125**, 11314–11328.

Gonzalez, A. & Nave, C. (1994). *Acta Cryst.* D**50**, 874–877.

Gonzalez, A., Thompson, A. & Nave, C. (1992). *Rev. Sci. Instrum.* **67**, 3356.

Gould, R. F. (1968). Editor. *Radiation Chemistry*, Vol. 1, *Advances in Chemistry Series*, No. 81, pp. 1–23. Washington, DC: American Chemical Society.

Halliwell, B. & Gutteridge, J. M. C. (1999). *Free Radicals in Biology and Medicine*, 3rd ed. Oxford: Oxford Science Publications.

Henderson, R. (1990). *Proc. R. Soc. London Ser. B*, **241**, 6–8.

Hope, H. (1988). *Acta Cryst.* B**44**, 22–26.

Jones, G. D. D., Lea, J. S., Symons, M. C. R. & Taiwo, F. A. (1987). *Nature (London)*, **330**, 772–773.

Kauffmann, B., Weiss, M. S., Lazmin, V. S. & Schmidt, A. (2006). *Structure*, **14**, 1099–1105.

Lagercrantz, C. (1971). *J. Phys. Chem.* **75**, 3466–3475.

Massover, W. (2006). *J. Synchrotron Rad.* **14**, 116–127.

Murray, J. W. (2004). DPhil thesis. Oxford University, UK.

Murray, J. W. & Garman, E. F. (2002). *J. Synchrotron Rad.* **9**, 347–354.

Neta, P., Huie, R. & Ross, A. B. (1988). *J. Phys. Chem. Ref. Data*, **17**, 1027–1284.

O'Neill, P., Stevens, D. L. & Garman, E. F. (2002). *J. Synchrotron Rad.* **9**, 329–332.

Owen, R. L., Rudiño-Piñera, E. & Garman, E. F. (2006). *Proc. Natl. Acad. Sci.* **103**, 4912–4917.

Petrik, N. G. & Kimmel, G. A. (2003). *Phys. Rev. Lett.* **90**, 166102-1–166102-4.

Powers, E. L., Ehret, C. F. & Bannon, A. (1957). *Appl. Microbiol.* **5**, 61.

Prutz, W. A., Butler, J., Land, E. J. & Swallow, A. J. (1989). *Int. J. Radiat. Biol.* **55**, 539–556.

Rao, D. N., Symons, M. C. R. & Stephenson, J. M. (1983). *J. Chem. Soc. Perkin Trans. II*, pp. 727–730.

Rao, P. S. & Hayon, E. (1974). *J. Phys. Chem.* **78**, 1193–1196.

Ravelli, R. B. G. & McSweeney, S. (2000). *Structure*, **8**, 315–328.

Ravelli, R. B. G., Murray, J. W., McGeehan, J., Owen, R. L., Cipriania, F., Theveneau, P., Weik, M. & Garman, E. F. (2007). In preparation.

Rodgers, D. W. (1997). *Methods in Enzymology*, edited by C. W. Carter Jr and R. M. Sweet, Vol. 276, pp. 183–203. London: Academic Press.

Sarma, R. & Zaloga, G. (1975). *J. Mol. Biol.* **98**, 479–484.

Sonntag, J. von, Mvula, E., Hildenbrand, K. & von Sonntag, C. (2004). *Chem. Eur. J.* **10**, 440–451.

Swartz, H. M. & Swartz, S. M. (1983). *Methods Biochem. Anal.* **29**, 207–323.

Symons, M. C. R. (1999). *Prog. React. Kinet. Mech.* **24**, 139–164.

Ward, J. F. (1988). *Prog. Nucl. Acid Res. Mol. Biol.* **35**, 95–125.

Weik, M., Bergés, J., Raves, M. L., Gros, P., McSweeney, S., Silman, I., Sussman, J. L., Houee-Levin, C. & Ravelli, R. B. G. (2002). *J. Synchrotron Rad.* **9**, 342–346.

Weik, M., Ravelli, R. B. G., Kryger, G., McSweeney, S., Raves, M. L., Harel, M., Gros, P., Silman, I., Kroon, J. & Sussman, J. L. (2000). *Proc. Natl. Acad. Sci. USA*, **97**, 623–628.

Zaloga, G. & Sarma, R. (1974). *Nature (London)*, **251**, 551–552.

Zbikowska, H. M., Nowak, P. & Wachowicz, B. (2006). *Free Radical Biol. Med.* **40**, 536–542.